Gaussian Process Monitoring of Layerwise-dependent Imaging Data

Runsang Liu[1], Bryan D. Vogt[2] and Hui Yang[1,*], *Senior Member, IEEE*

***Abstract*—Additive Manufacturing (AM) enables the direct production of complex geometries from computer-aided designs (CAD). The AM fabrication process is often executed in a layer-by-layer manner, whereby minute printing errors in one layer can manifest significant defects in the final part. In-situ quality monitoring and control are currently limited for AM processes and cause low repeatability. Recently. advanced imaging is increasingly invested in AM and leads to the proliferation of layerwise imaging data, which provides an opportunity to transform quality control of AM from post-build inspection to *in-situ* quality monitoring. However, existing methodologies for in-situ inspection primarily focus on key characteristics of image profiles that tend to be limited in the ability to analyze the variance components, as well as root causes and failure patterns that are critical to process improvement. This paper presents an Additive Gaussian Process with dependent layerwise correlation (AGP-D) to model the spatio-temporal correlation of layerwise imaging data for AM quality monitoring. The AGP-D consists of three independent GP modules. The first GP approximates the base profile, whereas the second and third GP capture the correlation within the same layer and among layers, respectively. Based on posterior predictions of new layers, Hotelling T^2 and generalized likelihood ratio (GLR) control tests are formulated to detect process shifts in the newly fabricated layer and analyze root causes. The proposed methodology is evaluated and validated using both simulation data and real-world case study of a cylinder build fabricated by a laser powder bed fusion (LPBF) machine. Experimental results show the proposed AGP-D is effective for real-time modeling and monitoring of layerwise-correlated imaging data.**

***Index Terms*: Additive manufacturing, Gaussian process, process control, statistical monitoring, spatiotemporal correlation**.

I. Introduction

FROM the advances in 3D printing that have led to surging demand for prototyping and on-demand fabrication, modern industry is shifting to a next-generation manufacturing paradigm that is highly adaptive and flexible to customized designs. Additive Manufacturing (AM) is an enabling technology for the direct transition of digital designs to functional 3-dimensional parts via layer-upon-layer deposition of materials. This, in turn, enables the creation of complex shapes that are otherwise difficult, or even impossible, to construct by traditional manufacturing technologies, e.g., subtractive manufacturing, with the added advantage of shorter lead times and the ability to customize on the fly. Therefore, AM overcomes conventional design and manufacturing constraints, especially for designs that involve complex geometries. Traditional post-build inspection uses optical methods such as scanning laser optical tomography (SLOT) to detect potential quality issues in finalized builds [1]. On the other hand, sensor-based monitoring allows manufacturers to find misprints and respond quickly to alleviate potential greater problems, reducing scraps and reworks. However, real-time quality control is usually limited for AM processes [2][3]. As a result, widespread application of AM is hampered by the yield and broad distribution in performance metrics, which can arise from the accumulation of minor errors during the print. As such, advanced sensing (e.g., optical or thermal imaging) is increasingly adopted to increase information visibility during AM processes, where well-placed sensing units capture and convert real-time process information into imaging data.

Although the availability of layerwise imaging data provides an opportunity to shift quality control of AM from post-build inspection to *in-situ* process monitoring, new analytical tools are urgently needed to extract useful information from imaging data and analyze stochastic variations in AM processes. Traditional statistical process control (SPC) measures the variability of a process using a large number of parts manufactured from the same design. However, AM is often used for prototyping and customization, thus it is not uncommon that only a few identical parts are fabricated. The poor repeatability in quality measurements poses significant challenges to conventional quality monitoring practices for AM processes. As shown in Fig. 1(a)-(c), SPC has achieved success in automotive and semiconductor industries in the past few decades. SPC methods have evolved from monitoring univariate features, multiple quality measurements to functional profiles. Nonetheless, traditional SPC is currently limited in the ability to model and analyze high-dimensional data [4], for example, layerwise imaging data as in Fig. 1(d). This, in turn, calls upon the development of new image-guided SPC methods.

Manuscript received: February 8th, 2021; Revised: April 12th, 2021; Accepted: June 13th, 2021.

This paper was recommended for publication by Editor Dana Kulic upon evaluation of the Associate Editor and Reviewers' comments.

The authors would like to thank National Science Foundation (NSF) CMMI-2011289 for supporting this work.

[1]R. Liu and H. Yang* are with the Complex Systems Monitoring, Modeling and Control lab, The Pennsylvania State University, University Park, PA, 16802 USA (*corresponding author: huy25@psu.edu).

[2]B. D. Vogt is with the Department of Chemical Engineering, The Pennsylvania State University, University Park, PA, 16802 USA (e-mail: bdv5051@psu.edu).

Digital Object Identifier (DOI): see top of this page

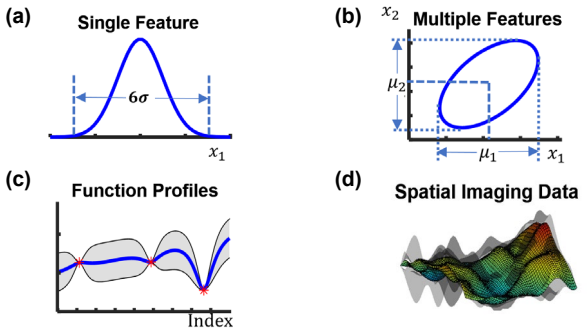

Fig. 1. The evolution of statistical process control (SPC) from (a) Univariate monitoring; (b) Joint monitoring of multiple features; (c) Function profile monitoring; to (d) high-dimensional imaging data.

Commonly, layerwise imaging data involve complex structures, within-layer and across-layer correlated variations. Real-world uncertainty in layerwise finishes of the build leads to stochastic variations in each image profile. Feature-based methods such as linear transformations [5][6], deep learning [7][8], multifractal analysis [9], and community-based statistics [10] are proposed to extract key characteristics and features from image profiles for statistical monitoring of manufacturing processes. However, feature-based methods tend to focus on one or more aspects of the engineering intent (e.g., the plume size, average temperature from melt pool images), as opposed to modeling the image profile as a random function. As a result, features are limited in the ability to analyze different types of variance components, as well as root causes and out-of-control patterns that are critical to process improvement.

These shortcomings have driven the design of alternative model-based methods. For example, parametric functions [11][12] are first proposed to approximate the profile and then monitor the parameter vector. To further increase the model performance, non-parametric models such as Gaussian Process (GP) [13] and spline modeling [14] are proposed and utilized. Among popular non-parametric models, GP is more favorable due to several key advantages. First, GPs have been demonstrated to successfully model complex profiles [15][16]. Second, GPs are flexible enough to be extended to higher input dimensions when compared to other non-parametric approaches. Third, stochastic GPs and posterior predictions allow a natural transition to the design of new SPC methods. With these advantages, several GP models have been proposed to model and analyze manufacturing data. For example, composite GP is used to model the smoothness of titanium alloy pieces [17], while additive GP with independent layers (AGP-I) uses two GPs to model the variation of wafer thickness profiles [13]. However, most existing model-based methods focus on the modeling of imaging data with an assumption of layerwise independence and are not developed to fully address layerwise correlation of imaging data from AM fabrication processes.

This paper presents an Additive Gaussian Process with dependent layerwise correlation (AGP-D) to characterize the spatio-temporal correlation of layerwise imaging data for real-time quality monitoring of AM fabrications. The AGP-D consists of three independent GP modules. The first GP approximates the base profile, whereas the second and third GPs capture the correlation within the same layer and across different layers. Based on posterior distributions of the new layer from AGP-D modeling, Hotelling T^2 and generalized likelihood ratio (GLR) tests are formulated to detect process deviations in a newly fabricated layer and analyze root causes. A real-time monitoring framework that combines the AGP-D model and multivariate control charts is also developed to enable *in-situ* quality monitoring of layerwise imaging data from AM fabrication procedures. The proposed methodology is evaluated and validated using simulation studies and a real-world case study of a cylinder build fabricated by a laser powder bed fusion (LPBF) machine. Experimental results show the proposed AGP-D and multivariate control charts are effective for real-time monitoring of layerwise-correlated imaging data.

This paper is organized as follows: Section II provides a literature review on relevant methods of image-based quality monitoring. Section III presents the proposed AGP-D and statistical monitoring methodology. Section IV shows the detailed experimental design and results using both simulations and a real-world case study. Section V discusses and concludes this study.

II. Research Background

Quality control in AM remains an enduring challenge despite advancements in sensing technology and SPC methods. Slight changes in process conditions can cause non-negligible impacts on the quality of AM builds [18]. As a result, image-guided monitoring that utilizes the selection of the cameras to provide opportunities for real-time process data is among the highest priorities for AM quality control. For example, infrared cameras detect thermal signals of layerwise builds to provide temperature history information, and can further be utilized to detect material discontinuities [19][20]. High-resolution cameras with multiple flash modules that enable immediate layer imaging after recoating and laser exposure are used to identify common defects such as porosities and poor surface finishes [21]. These sensors bring a wealth of high-dimensional imaging data that can further enable shape analysis on the print, for example, height, trajectory, and textures [22]. The plethora of process information necessitates the development of new analysis tools and SPC methods.

The imaging data stream collected by advanced cameras during manufacturing processes usually contains linear, nonlinear, and irregular information [23]. Therefore, feature-based methods focus on monitoring aggregated attributes extracted from layerwise imaging data. For example, principal component analysis (PCA) [5], Fourier transforms [6] and Pearson correlation coefficient (PCC) [24] can be used to extract linear features, while nonlinear and irregular features can be characterized using deep learning [7], and multifractal analysis [9], respectively. Low-rank tensor decomposition techniques are also used to extract key characteristic features

from high-dimensional image profiles [25]. Note that features extracted from thermal images such as plume size and average temperature of melt pool images are investigated to monitor the stability of melting conditions [26]. Active contours are also extracted for the characterization of layerwise images, where the plane-wise deviations are monitored by computing the distance between the nominal and the extracted contour [27]. Although feature-based approaches are shown to have certain advantages, very little has been done to model the image profile as a random function. Traditional feature-based approaches focus on the extraction of features from image profiles (e.g., infrared or optical images), while Gaussian process modeling is an alternative approach to model the image profile as a random function. The present investigation focuses on three random components in each layerwise image, i.e., (i) the base profile, (ii) within-layer, and (iii) across-layer correlated components that capture correlated deviations within the same layer and between different layers. Then, in-situ monitoring is formulated as a hypothesis testing problem, instead of classification or clustering problems with multiple feature descriptors. The development of alternative strategies for monitoring AM processes with layerwise images is useful due to distinct advantages and disadvantages of these methodologies.

Therefore, model-based approaches such as splines monitoring [14], support vector regression [28], and GP [13] have been proposed to estimate and characterize spatial image profiles. In addition, deep learning is not only used to extract features but also to predict material continuity based on the signatures developed from multiple cameras [8]. Among popular non-parametric models, GPs have gained noticeable attention for modeling complex patterns due to their flexibility and versatility. GPs are demonstrated to successfully model and predict complex profiles such as turbulent flows [29], liquefaction triggering procedures [30], heterogeneous land data in remote sensing [31]. In addition, GP was used to model complex shape and free-form surfaces of 3D point cloud data from a laser scanner [32]. Therefore, several GP models and their variants are being used to model profiles from manufacturing processes. For example, a series of GP models are used to model the polishing stages on a titanium alloy workpiece [17]. Additive GP with independent layers [13] is proposed to model and monitor the silicon wafer thickness profile considering both standard thickness and correlation in the measurement locations within the same wafer. However, most of existing model-based methods are mainly focused on modeling within-layer correlations and assume layerwise independence but are less concerned about across-layer correlated variations among imaging data in the process of AM fabrication. The ability to delineate within-layer and across-layer correlated components is critical to quality monitoring of AM fabrication processes in a layer-by-layer fashion and further mitigate incipient defects.

III. Research Methodology

In this section, we propose an online framework of AM process monitoring based on imaging data. As shown in Fig. 2, in-control layerwise imaging data are first pre-processed to create the stack of region of interests (ROIs) to focus on the fabrication area in the AM build and exclude nuisance information in the background area of powders. Next, the AGP-D model is trained on the in-control ROIs to model the imaging data in terms of the base profile, within and across layer correlations. The trained AGP-D model is then used to obtain the posterior distribution of pixel intensities in a new image profile. Finally, Hotelling T^2 and generalized likelihood ratio (GLR) tests are performed to detect process changes and/or variations based on confidence intervals from posterior distributions in the ROI of the newly fabricated layer. If the new layer is in-control, it is added to the training data and the AGP-D model is updated. Otherwise, *in-situ* rectification actions should be taken, where the choice of corrective actions can be determined via a sequential optimization framework as discussed in [33].

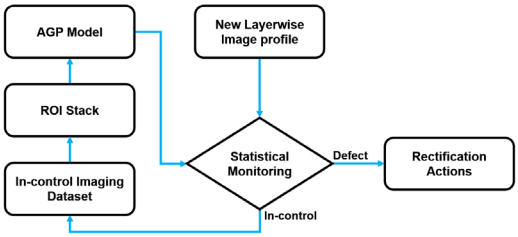

Fig. 2. Flow diagram of the proposed methodology

3.1 Additive Gaussian Process (AGP-D) Modeling

The stream of layerwise imaging data involves complex data structures and stochastic variations, which call upon the development of new analytical models for AM process monitoring. In particular, the sum of layerwise deviations is of interest, as well as mean functions and covariance functions. This motivates the development of new Gaussian process models to represent layerwise deviations as random functions. Note that the proposed model specifically takes across-layer correlations into consideration, which explicitly assumes that there is dependence in the deviations between layerwise image profiles. Let $x_{ij}^{(l)}$ be the $(i,j)^{th}$ pixel location of the l^{th} ROI, and $y_{ij}^{(l)}$ be the pixel intensity at the corresponding location. Fig. 3 shows layerwise image profiles are not independent of each other. Rather, two major types of correlation (within-layer and across-layer correlation) impact the distribution of intensities in the imaging data, which we refer to as the spatio-temporal correlation. Therefore, the distribution of the intensities is modeled as the sum of three

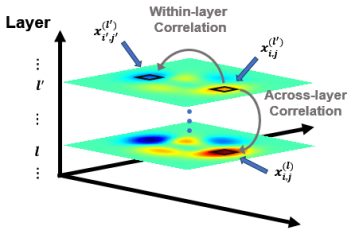

Fig. 3. Within-layer and across-layer correlation in layerwise ROIs.

independent functions:

$$y_{ij}^{(l)} = b\left(x_{ij}^{(l)}\right) + c_{wl}\left(x_{ij}^{(l)}\right) + c_{al}\left(x_{ij}^{(l)}\right) + \varepsilon \quad (1)$$

where $\varepsilon \sim N(0, \sigma_n^2)$ is the observation noise, $b \sim GP(\mathbf{m}_b, \mathbf{K}_b)$ is a realization of the base profile with mean $\mathbf{m}_b$ and covariance matrix $\mathbf{K}_b$, $c_{wl} \sim GP(0, \mathbf{K}_{wl})$ and $c_{al} \sim GP(0, \mathbf{K}_{al})$ capture within and across layer correlation, with zero mean and covariance matrices $\mathbf{K}_{wl}, \mathbf{K}_{al}$, accordingly. In this paper, we use the squared exponential covariance function, therefore the covariance matrix can be computed as:

$$\mathbf{K}\left(x_{ij}, x_{i'j'}\right) = \sigma^2 \exp\left[-\left(x_{ij} - x_{i'j'}\right)^T diag^{-1}(a)\left(x_{ij} - x_{i'j'}\right)\right] \quad (2)$$

where σ is the standard deviation and a is the length-scale that quantifies the correlation neighborhood. The base profile mathematically describes the standard geometric profile. The within-layer component $\mathbf{c}_{wl} \sim GP(0, \mathbf{K}_{wl})$ only contains the covariance within the same layer and the across-layer component $\mathbf{c}_{al} \sim GP(0, \mathbf{K}_{al})$ only contains covariance across different layers. The formulations of covariance structures grant each component to capture different patterns within the imaging data. Please note that covariance structures $\mathbf{K}_{wl}, \mathbf{K}_{al}$ are defined differently as follows:

$$\boldsymbol{K}_{wl}\left(x_{ij}^{(l)}, x_{i'j'}^{(l)}\right) = \sigma_{wl}^2 exp\left[-\left(x_{ij}^{(l)} - x_{i'j'}^{(l)}\right)^T diag^{-1}(a_{wl})\left(x_{ij}^{(l)} - x_{i'j'}^{(l)}\right)\right] \quad (3)$$

$$\boldsymbol{K}_{al}\left(x_{ij}^{(l)}, x_{i'j'}^{(l')}\right) = \sigma_{al}^2 exp\left[-\left(x_{ij}^{(l)} - x_{i'j'}^{(l')}\right)^T diag^{-1}(a_{al})\left(x_{ij}^{(l)} - x_{i'j'}^{(l')}\right)\right] \quad (4)$$

The three functions are assumed to be independent of each other. As a result, the observed pixel intensity $y_{ij}^{(l)}$ is essentially the sum of three GPs, i.e., $y_{ij}^{(l)} \sim GP(\mathbf{m}_b, \mathbf{K}_b + \mathbf{K}_{wl} + \mathbf{K}_{al})$, which we refer to as the AGP-D model. Assume the ROI stack of image profiles has the dimension of $N_p = n_x \times n_y \times L$, where n_x, n_y are the number of pixels in x, y directions and L is the number of layers. The linearized in-control location data become $\mathbf{X} = \left[x_{11}^{(1)}, \ldots x_{11}^{(2)}, \ldots x_{n_x n_y}^{(L)}\right]^T$ and pixel intensities are $\mathbf{y} = \left[y_{11}^{(1)}, \ldots y_{11}^{(2)}, \ldots y_{n_x n_y}^{(L)}\right]^T$, which has the dimension of $N_p \times 3$ and $N_p \times 1$, respectively. Let $\boldsymbol{\beta} = [\boldsymbol{\theta}_b, \boldsymbol{\theta}_{wl}, \boldsymbol{\theta}_{al}]$, where $\boldsymbol{\theta} = [\mu, \sigma^2, a]$, be the set of all hyperparameters in the AGP-D model, and $\widehat{\boldsymbol{\mu}}_{\mathbf{y}}$ be the mean estimates of in-control pixel intensities. The estimator $\widehat{\boldsymbol{\beta}}$ for the set of hyperparameters can be computed by maximizing the log-likelihood function:

$$\begin{aligned}\widehat{\boldsymbol{\beta}} = \arg\max_{\boldsymbol{\beta}} \Big\{ & -\frac{1}{2}\log(\det \mathbf{K}(\mathbf{X}, \mathbf{X})) \\ & -\frac{1}{2}\left(\mathbf{y} - \widehat{\boldsymbol{\mu}}_{\mathbf{y}}\right)^T \times \left(\mathbf{K}(\mathbf{X}, \mathbf{X})\right)^{-1} \\ & \times \left(\mathbf{y} - \widehat{\boldsymbol{\mu}}_{\mathbf{y}}\right)\Big\}\end{aligned} \quad (5)$$

In-control dataset is used to estimate the hyperparameters for each component in the AGP-D model by maximizing the log-likelihood function using a conjugate gradient optimizer. This study does not assume that all previous layers are normal. Commonly, defects can occur right at the beginning of the fabrication, or in the middle, or at the final phase. Type II errors can lead to the biased estimation of defective probability in a new layer. If accumulated, defective layers can be potentially mixed into in-control training dataset and thereby decrease the power of the proposed GP models. In the general practice, practitioners may opt to manually inspect and choose zero-defect layers (ROIs) to establish in-control training dataset. The model can only be updated with the addition of new layers that are closely inspected to be in-control. Although manual inspection is labor-intensive, practitioners can also opt to automatically update the model with new layers that are identified by the model to achieve a high probability to be in-control. Also, note that the computation of covariance function and model update is based on the majority of in-control datasets, instead of a single layer that may be defective.

Next, the AGP-D model is used to characterize the layerwise image profiles and compute the confidence bounds of the surface finish in the next layer, which provides a baseline to monitor the ROI in newly fabricated layers. Specifically, the marginal distribution of pixel intensity $\mathbf{y}^* = \mathbf{y}^{(L+1)}$ at location $\mathbf{X}_*$ in the newly collected image ROI is expected to follow a joint multivariate Gaussian distribution with the prior distribution:

$$\begin{bmatrix}\mathbf{y} \\ \mathbf{y}^*\end{bmatrix} \mid \mathbf{X}, \mathbf{X}_* \sim \mathcal{N}\left(\begin{bmatrix}\widehat{\boldsymbol{\mu}}_{\mathbf{y}} \\ \widehat{\boldsymbol{\mu}}_{\mathbf{y}^*}\end{bmatrix}, \begin{bmatrix}\mathbf{K}(\mathbf{X}, \mathbf{X}) & \mathbf{K}(\mathbf{X}, \mathbf{X}_*) \\ \mathbf{K}(\mathbf{X}_*, \mathbf{X}) & \mathbf{K}(\mathbf{X}_*, \mathbf{X}_*)\end{bmatrix}\right) \quad (6)$$

with the posterior distribution to be:

$$\mathbf{y}^* | \mathbf{y}, \mathbf{X}, \mathbf{X}_* \sim \mathcal{N}(\widehat{\boldsymbol{\mu}}_*, \widehat{\boldsymbol{\Sigma}}_*) \quad (7)$$

and the corresponding mean and covariance:

$$\widehat{\boldsymbol{\mu}}_* = \widehat{\boldsymbol{\mu}}_{\mathbf{y}^*} + \mathbf{K}(\mathbf{X}_*, \mathbf{X})(\mathbf{K}(\mathbf{X}, \mathbf{X}) + \sigma_n^2 \mathbf{I})^{-1}\left(\mathbf{y} - \widehat{\boldsymbol{\mu}}_{\mathbf{y}}\right) \quad (8)$$

$$\widehat{\boldsymbol{\Sigma}}_* = \mathbf{K}(\mathbf{X}_*, \mathbf{X}_*) - \mathbf{K}(\mathbf{X}_*, \mathbf{X})(\mathbf{K}(\mathbf{X}, \mathbf{X}) + \sigma_n^2 \mathbf{I})^{-1}\mathbf{K}(\mathbf{X}, \mathbf{X}_*) \quad (9)$$

where $\widehat{\boldsymbol{\mu}}_{\mathbf{y}}, \widehat{\boldsymbol{\mu}}_*$ are mean estimates from in-control and newly collected ROIs. Therefore, the intensity distribution from the new image ROI is expected to follow a multivariate Gaussian distribution with mean $\widehat{\boldsymbol{\mu}}_*$ and covariance $\widehat{\boldsymbol{\Sigma}}_*$. Although Gaussian Process is computationally expensive when the input dimension is large, there are serval ways to increase the computational efficiency. For example, fully independent training conditional (FITC) approximates covariance matrices using a smaller set of inducing inputs for a faster prediction. Block-wise matrix inversion allows a more efficient update of the AGP-D model after a new layer is regarded as normal and then added to the in-control training dataset. In addition, statistical sampling reduces the dimensionality of the input, thereby enabling a faster computation of GP modeling. Notably, statistical sampling in Gaussian process is different from feature selection. Feature-based approaches focus on the extraction of features from image profiles (e.g., infrared or optical images) based on one or more aspects of the engineering intent (e.g., the plume size from melt pool images). On the other hand, Gaussian process modeling is an alternative approach to model the image profile as a random function, where statistical samples help estimate covariance structures and then model the posterior distribution of image profiles.

3.2 Statistical Monitoring of Correlated Imaging Data

The AGP-D model provides real-time mean and variance estimation of intensity distribution of the ROI in newly fabricated layers. Therefore, hypothesis tests can be created

to test whether the new layer is out-of-control. Equation (7) shows that the posterior distribution follows a multivariate Gaussian distribution with the estimated mean vector $\widehat{\boldsymbol{\mu}}_*$ and covariance matrix $\widehat{\boldsymbol{\Sigma}}_*$. As such, the hypothesis to test whether a new layer is in-control or defective can be formulated as:

$$\begin{cases} H_0: \mathbf{y}^{(L+1)} \sim \mathcal{N}\left(\boldsymbol{\mu}_*{}^{(L+1)}, \boldsymbol{\Sigma}_*^{(L+1)}\right) \\ H_1: \mathbf{y}^{(L+1)} \nsim \mathcal{N}\left(\boldsymbol{\mu}_*{}^{(L+1)}, \boldsymbol{\Sigma}_*^{(L+1)}\right) \end{cases} \tag{10}$$

where $\boldsymbol{\mu}_*{}^{(L+1)}$ is the true mean vector, $\boldsymbol{\Sigma}_*^{(L+1)}$ is the true covariance matrix, and $L+1$ is the layer index of a newly fabricated layer. Traditionally, the χ^2 statistic is often to perform this hypothesis testing when the population mean and covariance are known:

$$\chi^2_{L+1} = \left(\mathbf{y}^{(L+1)} - \boldsymbol{\mu}_*{}^{(L+1)}\right)^T \left(\boldsymbol{\Sigma}_*^{(L+1)}\right)^{-1} \left(\mathbf{y}^{(L+1)} - \boldsymbol{\mu}_*{}^{(L+1)}\right) \tag{11}$$

The upper control limit is $UCL = \chi^2(n^{(L+1)}, \alpha)$, where α is the significance level. Because the chi-square statistic is the squared term between the observational and true mean vector, the lower control limit is zero. The null hypothesis is rejected, if the test statistic is beyond the upper control limit. However, the population mean $\boldsymbol{\mu}_*{}^{(L+1)}$ and covariance $\boldsymbol{\Sigma}_*^{(L+1)}$ are often unknown and need to be estimated from the in-control data as $\widehat{\boldsymbol{\mu}}_*$ and $\widehat{\boldsymbol{\Sigma}}_*$. If we replace $\boldsymbol{\mu}_*{}^{(L+1)}$ and $\boldsymbol{\Sigma}_*^{(L+1)}$ in χ^2_{L+1} with estimated sample mean $\widehat{\boldsymbol{\mu}}_*$ and covariance $\widehat{\boldsymbol{\Sigma}}_*$, the test statistic in equation (11) becomes:

$$T^2_{L+1} = \left(\boldsymbol{y}^{(L+1)} - \widehat{\boldsymbol{\mu}}_*{}^{(L+1)}\right)^T \left(\widehat{\boldsymbol{\Sigma}}_*^{(L+1)}\right)^{-1} \left(\boldsymbol{y}^{(L+1)} - \widehat{\boldsymbol{\mu}}_*{}^{(L+1)}\right) \tag{12}$$

which is called the Hotelling T^2 statistic that is commonly used to test the hypothesis as equation (10) in the literature. In practice, control limits of the T^2 statistic can be approximated by a chi-square distribution with $n^{(L+1)}$ degrees of freedom, therefore, the null hypothesis is rejected when the T^2 statistic is larger than $\chi^2(n^{(L+1)}, \alpha)$.

The Hotelling T^2 test is designed to detect changes and shifts in the AM processes. However, it is also imperative to further perform the root cause analysis. In the practice, the generalized likelihood ratio (GLR) test is often used to detect the process changes and further perform root cause diagnosis. Specifically, if the manufacturing process is out of control, the deviation is captured by the root cause component γ:

$$\begin{aligned} y_{ij}^{(L+1)} = {} & b\left(x_{ij}^{(L+1)}\right) + c_{wl}\left(x_{ij}^{(L+1)}\right) \\ & + c_{al}\left(x_{ij}^{(L+1)}\right) + \gamma\left(x_{ij}\right) + \varepsilon \end{aligned} \tag{13}$$

where $\gamma(x_{ij})$ denotes the deviation due to assignable causes in the out-of-control process that is characterized by hyperparameter $\boldsymbol{\theta}_\gamma = [\mu_\gamma, \sigma_\gamma^2, a_\gamma]$ to detect specific deviations in mean, variance, and roughness. Although the base profile remains the same, γ adds another degree of mean profile variations if there is any. This, in turn, offers the flexibility to model layers with different mean profiles and identify root causes. The hypothesis to test whether $\gamma(\cdot)$ is significantly different from zero can be formulated as:

$$\begin{cases} H_0: \mathbf{y}^{(L+1)} \sim \mathcal{N}\left(\widehat{\boldsymbol{\mu}}_*{}^{(L+1)}, \widehat{\boldsymbol{\Sigma}}_*^{(L+1)}\right) \\ H_1: \mathbf{y}^{(L+1)} \sim \mathcal{N}\left(\widehat{\boldsymbol{\mu}}_*{}^{(L+1)} + \boldsymbol{\mu}_\gamma, \widehat{\boldsymbol{\Sigma}}_*^{(L+1)} + \boldsymbol{\Sigma}_\gamma\right) \end{cases} \tag{14}$$

As such, the hypothesis can be reformulated as: $H_0: \boldsymbol{\theta}_\gamma = 0$, $H_1: \boldsymbol{\theta}_\gamma \neq 0$ to test whether there are shifts in model parameters. Then, the GLR statistic can be computed as:

$$R_{L+1} = 2\ln \frac{\underset{\boldsymbol{\theta}_\gamma}{\operatorname{argmax}} \operatorname{Likelihood}(H_1)}{\operatorname{Likelihood}(H_0)} \tag{15}$$

which computes the ratio of likelihoods under H_0 and H_1, respectively. Under H_0, the likelihood is computed as:

$$\begin{aligned} &\operatorname{Likelihood}(H_0) = \\ &(2\pi)^{-\frac{n^{(L+1)}}{2}} \det\left(\widehat{\boldsymbol{\Sigma}}_*^{(L+1)}\right)^{-\frac{1}{2}} \exp\left[-\frac{1}{2}\left(\mathbf{y}^{(L+1)}\right.\right. \\ &\qquad \left.\left. - \widehat{\boldsymbol{\mu}}_*{}^{(L+1)}\right)^T \left(\widehat{\boldsymbol{\Sigma}}_*^{(L+1)}\right)^{-1} \left(\mathbf{y}^{(L+1)}\right. \right. \\ &\qquad \left.\left. - \widehat{\boldsymbol{\mu}}_*{}^{(L+1)}\right)\right] \end{aligned} \tag{16}$$

Similarly, the likelihood when H_1 is true is computed as:

$$\begin{aligned} &\operatorname{Likelihood}(H_1) = \\ &(2\pi)^{-\frac{n^{(L+1)}}{2}} \det\left(\widehat{\boldsymbol{\Sigma}}_*^{(L+1)} + \widehat{\boldsymbol{\Sigma}}_\gamma\right)^{-\frac{1}{2}} \exp\left[-\frac{1}{2}\left(\mathbf{y}^{(L+1)}\right.\right. \\ &\qquad \left.\left. - \widehat{\boldsymbol{\mu}}_*{}^{(L+1)} - \widehat{\boldsymbol{\mu}}_\gamma\right)^T \left(\widehat{\boldsymbol{\Sigma}}_*^{(L+1)}\right.\right. \\ &\qquad \left.\left. + \widehat{\boldsymbol{\Sigma}}_\gamma\right)^{-1} \left(\mathbf{y}^{(L+1)} - \widehat{\boldsymbol{\mu}}_*{}^{(L+1)} - \widehat{\boldsymbol{\mu}}_\gamma\right)\right] \end{aligned} \tag{17}$$

The GLR test rejects the null hypothesis H_0 when the test statistic $R_{L+1} > \frac{1}{2}(\chi^2(1,\alpha) + \chi^2(2,\alpha))$. When a defective layer is detected, hyperparameters in $\widehat{\boldsymbol{\theta}}_\gamma$ can be further utilized to diagnose process changes of a specific type, e.g., mean shift, variance change, or roughness change.

IV. Experimental Design and Results

In this investigation, we first evaluate and validate the effectiveness of the proposed AGP-D model, and statistical monitoring schemes using a simulation study. The simulation study aims to evaluate the effectiveness of layerwise correlated data estimation and further investigate the performance of statistical monitoring schemes under different types of process shifts. With the efficacy demonstrated using simulations, a real-world case study of a cylinder build from an LPBF machine is further conducted.

4.1 AGP-D Modeling Performance

We first show that the proposed AGP-D model is sufficient to estimate the surface finishes and capture the layerwise correlation from image profiles in AM processes using simulated data. In this simulation, we use the following sinusoid function to be the base profile:

$$f(x_1, x_2) = \cos(x_1) + \sin\left(\frac{x_1}{5}\right)\cos(x_2) \tag{18}$$

with $x_1 \in [-3,3]$ and $x_2 \in [-3,3]$. The within-layer and across-layer correlation are generated from two independent GPs with hyperparameter of: $\boldsymbol{\theta}_{wl} = [\mu_{wl} = 0, a_{wl} = (0.5,0.5,0.5), \sigma_{wl} = 1.5]$ and $\boldsymbol{\theta}_{al} = [\mu_{wl} = 0, a_{al} = (2,2,2.5), \sigma_{al} = 1.5]$, respectively. These simulated spatio-temporal correlations will result in a more realistic correlation across the layers. To generate the layerwise correlated data, we utilize the Cholesky factorization:

$$\mathbf{y} = \mathbf{f} + chol(\mathbf{K}) \times rnd + \boldsymbol{\varepsilon} \tag{19}$$

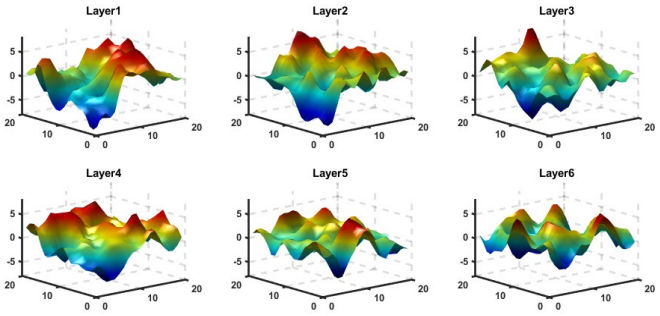

Fig. 4. Simulated layerwise-correlated data

where $\mathbf{K}$ is the covarance matrix, $rnd{\sim}Z(0,1)$ is the standard normal random variable, and $\boldsymbol{\varepsilon}{\sim}(0,1e-4)$ is the random noise.

As shown in Fig. 4, we generated in-control layers that have varying intensities over time, simulating the layerwise image profiles of AM build during layer-upon-layer fabrication procedures. We compare the proposed methodology with the original GP (OGP) with noisy measurements [34] and AGP-I (i.e., independent layerwise correlation) proposed in [13]. The hyperparameters for the three GP models are estimated using the maximum log-likelihood method, and a total of 400 randomly sampled data points are used to predict the prior distribution of the in-control profile. The negative log-likelihood (NLL) of the predicted distribution is used to quantify the performance of model estimation. Because we aim to estimate the distribution and then compute the confidence bounds of unseen layers, the likelihood that quantifies the goodness of fit of the model is more suitable than the commonly used root mean squared error (RMSE). NLL shows how well the model fits the data based on the likelihood of the fit, and a smaller NLL value indicates the model has a better fit.

As shown in Fig. 5 (a)-(c), the difference among mean predictions from AGP-D, AGP-I, and OGP is not significant, and all three methods predict the mean of the layer close to the simulated layer. Shown in Fig. 5 (d)-(f) is the estimated covariance structure, where the predicted covariance is overlaid with the simulated covariance to demonstrate the difference in covariance magnitude. The less gray area we can see, the better the prediction. As shown in Fig. 5 (d)-(f), the AGP-D and AGP-I have similar predicted covariance structures, only with minute differences. However, the OGP is limited in the ability to predict the simulated covariance

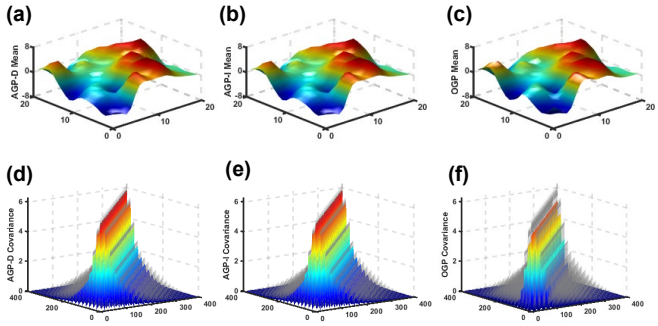

Fig. 5. Predicted means and covariances of the first layer using different GP models: (a) AGP-D (proposed) predicted mean; (b) AGP-I predicted mean; (c) OGP predicted mean; (d) AGP-D predicted covariance; (e) AGP-I predicted covariance and (f) OGP predicted covariance.

structure, leaving the largest area of shades. This is because the OGP did not take spatio-temporal correlations into consideration. Through our experiments, the AGP-D has an NLL of 532, while AGP-I and OGP has an NLL of 907 and 1647, respectively. This comparison demonstrates that although three models are equally effective in mean estimation, the proposed AGP-D is overall more effective to model layerwise correlated image profiles.

4.2 Performance comparisons of Monitoring Schemes

In this section, we examine the performance of the proposed statistical monitoring scheme under different types of defects. Based on engineering knowledge, three types of process-change scenarios are observed on the surface during layerwise fabrication: shift in mean, change in variance, and change in roughness. Therefore, we use an additional GP $\gamma(x_{ij})$ with mean μ_γ, variance σ_γ, and length scale a_γ to model the three types of shifts, correspondingly. Note that in the squared exponential covariance function mentioned in section III, when the length scale is increased, the covariance structure is flatter, hence the resulting deviation is smoother.

To investigate the performance of the proposed statistical monitoring schemes, we generated 6 layers using the same setting as in section 4.1, with the additional GP added to the 6^{th} layer to simulate process shifts. The first 5 layers are treated as in-control layers, while the proposed AGP-D model is utilized to predict the image profile of the 6^{th} layer. Both the GLR and T^2 tests are used to determine if the new layer conforms with the predicted distribution. The performance of the proposed statistical monitoring scheme is quantified with type II error under three types of process changes since type II error describes the occurrence of error when the test falsely accepts the null hypothesis, i.e., a layer is not defective. The control limits for both tests are computed based on the significance level $\alpha = 0.05$, and the proposed AGP-D model is benchmarked with AGP-I and OGP.

Fig. 6 shows the operation characteristic (OC) curves of different types of shifts under three different GP models. The OC curves show that both GLR and T^2 tests are capable to detect process changes. Specifically, all three GP models are

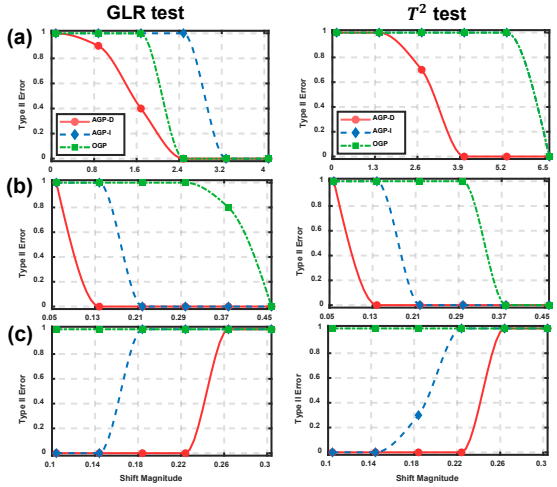

Fig. 6. Performance comparison of Type II errors from AGP-I, AGP-D, and OGP models in detecting different types and magnitudes of process shifts: (a) Mean shift; (b) Variance change and (c) roughness change.

capable to detect process shifts in terms of mean and variance, while OGP is limited in the ability to detect changes in roughness. This is because OGP does not consider correlations in layerwise imaging data. However, the AGP-D is shown to have a higher sensitivity in terms of detecting all three types of process changes when compared to the AGP-I and OGP models. Therefore, we conclude the proposed AGP-D yields a superior result when monitoring process changes in layerwise-correlated imaging data.

4.3 Real-world Case Study

To further evaluate the effectiveness of the proposed methodology, a real-world case study is conducted on the imaging dataset collected at Penn State CIMP-3D as shown in Fig. 7(a). The cylinder build is fabricated under a direct metal laser sintering (DMLS) process by an EOSINT M280 LPBF machine with a Titanium alloy material. Fig. 7(b) shows an example of the layerwise imaging data of the build, where each AM image contains 1000×1017 pixels.

Fig. 7. (a) The cylinder build; (b) a layerwise image of the build.

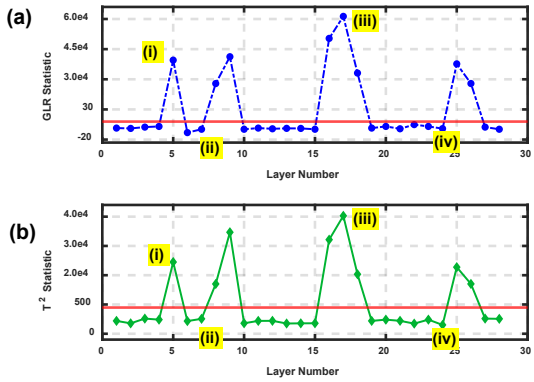

Fig. 8. (a) GLR and (b) T^2 control charts on layerwise imaging data of the cylinder build. The red line is the control limit computed using $\alpha = 0.05$. (i)-(iv) are examples of in-control and out-of-control layers.

The layerwise imaging data are first processed using image registration to obtain ROIs and eliminate background noises (e.g., powders). In this study, a total of 58 layerwise images are collected, where 30 of them are closely inspected to be defect free and are thus used as the training dataset. The rest 28 layers are used as testing data. To increase computational efficiency, a total of 1000 samples are drawn from the in-control ROI stack. Next, the proposed AGP model is trained on in-control ROIs and then predicts the posterior distribution of the newly collected ROI. Finally, for each new ROI, we use the proposed GLR and T^2 control chart to detect whether it is in-control or not.

Fig. 8 shows the variations of GLR and T^2 test statistics collected with respect to the index of testing layers. We can observe that 8 layers have a test statistic that significantly lies above the threshold, which is computed using significance level $\alpha = 0.05$. This indicates these 8 layers are tested to be defective. In addition, two statistical monitoring schemes have reached a consensus on the detection of out-of-control layers. To further investigate root causes of abnormal changes, we show examples of ROI from layers tested as defective and in-control in Fig. 9(i)-(iv). It may be noted that the porosity defects cause the nonconformity of intensity distributions which lead to a test statistic beyond the UCL. For the remaining layers, we can observe test results fluctuate but are still below the threshold, which indicates the process is in control. The average computation time for one layer is 5.39 seconds, while the minimum time to fabricate a layer is 28.12 seconds. The computation time is estimated with the use of a laptop computer with Intel Core i7 2.60GHz, 16GB RAM, and can be further improved with high-performance industrial computers. In our case study, the computational speed to update the AGP-D model is fast enough for the implementation of hypothesis testing and real-time monitoring objectives.

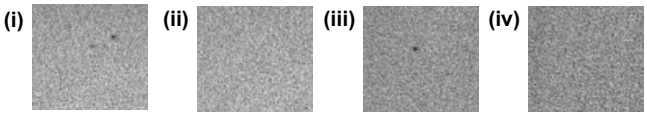

Fig. 9. Example images that are in-control (ii, iv) and defective (i, iii).

V. Discussion and Conclusions

Product quality is a key determinant for the broad adoption of new manufacturing technologies. Although AM has gained increasing attention due to its flexibility and capability to fabricate complex shapes, AM processes are currently limited in their *in-situ* quality monitoring, which poses challenges to the wide adoption of AM in commercial applications. With the rising investment by manufacturers in advanced sensing, real-time imaging data has now become available for quality monitoring. Such a plethora of high-dimensional imaging data necessitates the development of new image-guided SPC methods to effectively utilize the newfound data for real-time process control. Traditional image profile monitoring methods tend to focus on key characteristics (e.g., the plume size, average temperature from melt pool images), as opposed to modeling the image profile as a random function.

In this paper, we present a new Additive Gaussian Process model to characterize and model spatio-temporal correlations of layerwise imaging data for real-time quality monitoring of AM fabrications. The developed AGP-D represents each image profile with three stochastic components, i.e., the base profile, within-layer and across-layer correlation profiles. After training the AGP-D model with in-control imaging data, the posterior distribution of a newly fabricated layer is obtained, which is then incorporated into GLR and T^2 tests to detect process shifts. If the newly fabricated layer passes the hypothesis test, it is added to in-control dataset. Otherwise, correction actions shall be taken. The proposed methodology is evaluated and validated using both simulation studies and a real-world case study. Experimental results show that the proposed AGP-D has strong potentials for modeling layerwise imaging data in AM and further enabling in-situ quality monitoring.

Although this study focuses on the cylinder build, Gaussian processes are flexible enough to model complex shapes and free-form surfaces. It may be noted that shape-to-image registration between CAD drawings and layerwise profiles can be performed to delineate ROIs from the background noise (e.g., powder areas) and improve the model robustness. If a new layer has a different shape from previous layers, this actually does not impact the computation of covariance structures. Simply, the covariance matrix can be defined and computed within the ROI boundary. In other words, although the geometric boundary will generally vary between layers in an AM build, this will not impact the computation of the covariance matrix, nor the ability to model experimentally resolvable local minute variations in each individual layer.

REFERENCES

[1] G. Hohenhoff, H. Meyer, P. Jaeschke, T. Ripken, D. Kracht, and S. Kaierle, "Comparison of SLOT and μ -CT investigation of 3D printed polymer parts for quality assurance," *J. Laser Appl.*, vol. 32, no. 2, p. 022051, 2020.

[2] H. Yang *et al.*, "Six-Sigma Quality Management of Additive Manufacturing," *Proc. IEEE*, pp. 1–30, 2020.

[3] B. Yao, F. Imani, and H. Yang, "Markov decision process for image-guided additive manufacturing," *IEEE Robot. Autom. Lett.*, vol. 3, no. 4, pp. 2792–2798, 2018.

[4] G. Liu, C. Kan, Y. Chen, and H. Yang, "Model-driven parametric monitoring of high-dimensional nonlinear functional profiles," in *IEEE International Conference on Automation Science and Engineering*, pp. 722–727, 2014.

[5] K. Wang and W. Jiang, "High-dimensional process monitoring and fault isolation via variable selection," *J. Qual. Technol.*, vol. 41, no. 3, pp. 247–258, 2009.

[6] B. R. Wood, K. R. Bambery, C. J. Evans, M. A. Quinn, and D. McNaughton, "A three-dimensional multivariate image processing technique for the analysis of FTIR spectroscopic images of multiple tissue sections," *BMC Med. Imaging*, vol. 6, no. 12, pp. 1–9, 2006.

[7] F. Imani, R. Chen, E. Diewald, E. Reutzel, and H. Yang, "Deep learning of variant geometry in layerwise imaging profiles for additive manufacturing quality control," *J. Manuf. Sci. Eng. Trans. ASME*, vol. 141, no. 11, p. 111001, 2019.

[8] A. Gaikwad, B. Giera, G. M. Guss, J.-B. Forien, M. J. Matthews, and P. Rao, "Heterogeneous sensing and scientific machine learning for quality assurance in laser powder bed fusion – A single-track study," *Addit. Manuf.*, vol. 36, p. 101659, 2020.

[9] B. Yao, F. Imani, A. S. Sakpal, E. W. Reutzel, and H. Yang, "Multifractal Analysis of Image Profiles for the Characterization and Detection of Defects in Additive Manufacturing," *J. Manuf. Sci. Eng. Trans. ASME*, vol. 140, no. 3, p. 031014, 2018.

[10] C. Kan and H. Yang, "Dynamic network monitoring and control of in situ image profiles from ultraprecision machining and biomanufacturing processes," *Qual. Reliab. Eng. Int.*, vol. 33, no. 8, pp. 2003–2022, 2017.

[11] W. A. Jensen, J. B. Birch, and W. H. Woodall, "Monitoring correlation within linear profiles using mixed models," *J. Qual. Technol.*, vol. 40, pp. 167–183, 2008.

[12] C. Zou, C. Zhou, Z. Wang, and F. Tsung, "A self-starting control chart for linear profiles," *J. Qual. Technol.*, no. 39, pp. 364–375, 2007.

[13] L. Zhang, K. Wang, and N. Chen, "Monitoring wafers geometric quality using an additive Gaussian process model," *IIE Trans.*, vol. 48, no. 4, pp. 1–15, 2016.

[14] S. C. Chuang, Y. C. Hung, W. C. Tsai, and S. F. Yang, "A framework for nonparametric profile monitoring," *Comput. Ind. Eng.*, vol. 64, no. 1, pp. 482–491, 2013.

[15] L. Cheng *et al.*, "An additive Gaussian process regression model for interpretable non-parametric analysis of longitudinal data," *Nat. Commun.*, vol. 10, no. 1, p. 1798, 2019.

[16] F. Imani, C. Cheng, R. Chen, and H. Yang, "Nested Gaussian process modeling and imputation of high-dimensional incomplete data under uncertainty," *IISE Trans. Healthc. Syst. Eng.*, vol. 9, no. 4, pp. 315–326, 2019.

[17] S. Jin, A. Iquebal, S. Bukkapatnam, A. Gaynor, and Y. Ding, "A Gaussian Process Model-Guided Surface Polishing Process in Additive Manufacturing," *J. Manuf. Sci. Eng.*, vol. 142, no. 1, p. 011003, 2019.

[18] F. Imani, A. Gaikwad, M. Montazeri, P. Rao, H. Yang, and E. Reutzel, "Process mapping and in-process monitoring of porosity in laser powder bed fusion using layerwise optical imaging," *J. Manuf. Sci. Eng. Trans. ASME*, vol. 140, no. 10, p. 101009, 2018.

[19] E. Rodriguez, J. Mireles, C. A. Terrazas, D. Espalin, M. A. Perez, and R. B. Wicker, "Approximation of absolute surface temperature measurements of powder bed fusion additive manufacturing technology using in situ infrared thermography," *Addit. Manuf.*, vol. 5, pp. 31–39, 2015.

[20] M. Khanzadeh, S. Chowdhury, M. A. Tschopp, H. R. Doude, M. Marufuzzaman, and L. Bian, "In-situ monitoring of melt pool images for porosity prediction in directed energy deposition processes," *IISE Trans.*, vol. 51, no. 5, pp. 437–455, 2019.

[21] B. K. Foster, E. W. Reutzel, A. R. Nassar, B. T. Hall, S. W. Brown, and C. J. Dickman, "Optical, layerwise monitoring of powder bed fusion," in *Proceedings - 26th Annual International Solid Freeform Fabrication Symposium - An Additive Manufacturing Conference, SFF 2015*, 2015, pp. 295–307.

[22] A. L. Petsiuk and J. M. Pearce, "Open source computer vision-based layer-wise 3D printing analysis," *Addit. Manuf.*, vol. 36, p. 101473, 2020.

[23] F. Imani, B. Yao, R. Chen, P. Rao, and H. Yang, "Joint multifractal and lacunarity analysis of image profiles for manufacturing quality control," *J. Manuf. Sci. Eng. Trans. ASME*, vol. 141, no. 4, pp. 1–9, 2019.

[24] X. Zhang *et al.*, "Correlation approach for quality assurance of additive manufactured parts based on optical metrology," *J. Manuf. Process.*, vol. 53, pp. 310–317, 2020.

[25] H. Yan, K. Paynabar, and J. Shi, "Image-based process monitoring using low-rank tensor decomposition," *IEEE Trans. Autom. Sci. Eng.*, vol. 12, no. 1, pp. 216–227, 2015.

[26] M. Grasso, A. G. Demir, B. Previtali, and B. M. Colosimo, "In situ monitoring of selective laser melting of zinc powder via infrared imaging of the process plume," *Robot. Comput. Integr. Manuf.*, no. 49, pp. 229–239, 2018.

[27] L. Pagani, M. Grasso, P. J. Scott, and B. M. Colosimo, "Automated layerwise detection of geometrical distortions in laser powder bed fusion," *Addit. Manuf.*, no. 36, p. 101435, 2020.

[28] Y. C. Hung, W. C. Tsai, S. F. Yang, S. C. Chuang, and Y. K. Tseng, "Nonparametric profile monitoring in multi-dimensional data spaces," *J. Process Control*, vol. 22, no. 2, pp. 397–403, 2012.

[29] S. Mak *et al.*, "An Efficient Surrogate Model for Emulation and Physics Extraction of Large Eddy Simulations," *J. Am. Stat. Assoc.*, vol. 113, no. 254, pp. 1443–1456, 2018.

[30] M. W. Greenfield and A. Grant, "Probabilistic regional-scale liquefaction triggering modeling using 3D Gaussian processes," *Soil Dyn. Earthq. Eng.*, vol. 134, p. p106159, 2020.

[31] D. H. Svendsen, L. Martino, M. Campos-Taberner, F. J. Garcia-Haro, and G. Camps-Valls, "Joint Gaussian Processes for Biophysical Parameter Retrieval," *IEEE Trans. Geosci. Remote Sens.*, vol. 56, no. 3, pp. 1718–1727, 2018.

[32] E. del Castillo, B. M. Colosimo, and S. D. Tajbakhsh, "Geodesic Gaussian Processes for the Parametric Reconstruction of a Free-Form Surface," *Technometrics*, vol. 57, no. 1, pp. 87–99, 2015.

[33] B. Yao and H. Yang, "Constrained markov decision process modeling for sequential optimization of additive manufacturing build quality," *IEEE Access*, vol. 6, no. 1, pp. 54786–54794, 2018.

[34] W. Carl Edward, Rasmussen and C. K. I., *Gaussian Processes for Machine Learning*. Boston, MA: MITPress, 2006.